Flight Dynamics of an Aeroshell Using an Attached Inflatable Aerodynamic Decelerator

Erik Axdahl*
National Institute of Aerospace, Hampton, VA 23666

Juan R. Cruz† and Mark Schoenenberger‡
NASA Langley Research Center, Hampton, VA 23681

and

Alan Wilhite§
National Institute of Aerospace, Hampton, VA 23666

An aeroelastic analysis of the behavior of an entry vehicle utilizing an attached inflatable aerodynamic decelerator during supersonic flight is presented. The analysis consists of a planar, four degree of freedom simulation. The aeroshell and the IAD are assumed to be separate, rigid bodies connected with a spring-damper at an interface point constraining the relative motion of the two bodies. Aerodynamic forces and moments are modeled using modified Newtonian aerodynamics. The analysis includes the contribution of static aerodynamic forces and moments as well as pitch damping. Two cases are considered in the analysis: constant velocity flight and planar free flight. For the constant velocity and free flight cases with neutral pitch damping, configurations with highly-stiff interfaces exhibit statically stable but dynamically unstable aeroshell angle of attack. Moderately stiff interfaces exhibit static and dynamic stability of aeroshell angle of attack due to damping induced by the pitch angle rate lag between the aeroshell and IAD. For the free-flight case, low values of both the interface stiffness and damping cause divergence of the aeroshell angle of attack due to the offset of the IAD drag force with respect to the aeroshell center of mass. The presence of dynamic aerodynamic moments was found to influence the stability characteristics of the vehicle. The effect of gravity on the aeroshell angle of attack stability characteristics was determined to be negligible for the cases investigated.

Nomenclature

A	=	initial amplitude
B	=	decay constant
C_A	=	aerodynamic axial force coefficient
C_{m_α}	=	aerodynamic pitching moment coefficient slope about attachment point, $\partial C_m / \partial \alpha$
C_{m_Q}	=	aerodynamic pitch damping coefficient about attachment point, $\partial C_m / \partial (Qd/2V)$
C_{N_α}	=	aerodynamic normal force coefficient slope, $\partial C_N / \partial \alpha$
d	=	vehicle diameter
F_A	=	aerodynamic axial force
F_N	=	aerodynamic normal force
g	=	acceleration due to gravity

* Graduate Research Assistant, Georgia Institute of Technology, Axdahl@gatech.edu, Student Member AIAA
† Aerospace Engineer, Atmospheric Flight and Entry Systems Branch, Juan.R.Cruz@NASA.gov
‡ Aerospace Engineer, Atmospheric Flight and Entry Systems Branch, Mark.Schoenenberger-1@NASA.gov, Member AIAA
§ Professor, Georgia Institute of Technology, Wilhite@nianet.org, Associate Fellow AIAA

h = altitude
H = scale height
I_{yy} = mass moment of inertia about the body-fixed coordinate frame origin
I_{eff} = effective mass moment of inertia about the body-fixed coordinate frame origin
m = mass
$M_{aero,C}$ = total aerodynamic moment of the vehicle about point C
M_R = interface moment
Q = pitch rate
q_∞ = dynamic pressure
$q_{\infty,0}$ = initial dynamic pressure
R_x = axial interface force
R_z = normal interface force
S = vehicle reference area
t = time
u = axial velocity
$\mathbf{v}_C$ = velocity vector of the body-fixed coordinate frame origin
V = airspeed
w = normal velocity
x, z = body-fixed coordinate frame
x_{CM}, z_{CM} = axial and normal locations, respectively, of center of mass
X , Z = inertial coordinates

α = angle of attack
η = interface damping
$\hat{\eta}$ = non-dimensional interface damping
κ = interface stiffness
$\hat{\kappa}$ = non-dimensional interface stiffness
ω = angular frequency
ϕ = phase angle
ρ = atmospheric density
ρ_0 = surface atmospheric density
θ = pitch angle
$\Delta\theta$ = pitch difference between aeroshell and IAD

’ = superscript indication of IAD quantity

CL = Centerline
IAD = Inflatable Aerodynamic Decelerator
LH = Local Horizon

I. Introduction

The recent resurgence of research activities related to the development of inflatable aerodynamic decelerators (IAD) aims to create an enabling technology for global Martian surface access and the landing of large payloads, especially for vehicles with high ballistic coefficients. Although the beneficial drag characteristics of IADs are well-established,[1] the question of stability for various shapes has yet to be answered satisfactorily. Knowledge of the stability of an IAD is important for ensuring the vehicle remains within a tolerable range of rotation rates during flight. This study is a first-order analysis of the stability characteristics of a flexibly-connected aeroshell and IAD.

As the interface between the aeroshell and the IAD is flexible, an aeroelastic multibody simulation is required to capture the effect this flexibility has on the free flight stability characteristics of the system. This analysis is an aeroelastic study of a coupled, flexible aeroshell-IAD system in supersonic free flight. The development of the four

degree of freedom equations of motion is described along with the aerodynamics involved. Non-dimensional parameters are introduced to assist in the evaluation of the results. The simulation is validated in the rigid body limit with previously published rigid body simulations and with angle of attack amplitude growth theory.[2] Two flight regimes are studied using the simulation. The first is a constant velocity simulation where the gravity force is neglected and the vehicle is allowed to heave and rotate freely. The second case is that of a free flight simulation. Mechanisms are proposed to explain the stability behavior of the vehicle.

II. Modeling

A. Vehicle Definition

Figure 1 shows an aeroshell with an isotensoid attached IAD during atmospheric descent. Because the aftbody of the aeroshell is mostly enclosed by the IAD, only the geometry of the aeroshell forebody, a 70-degree sphere cone, is considered in this analysis for the purposes of aerodynamics. The IAD is a scaled version of an isotensoid shape analyzed and tested by Mikulas and Bohon.[3] The shape is axisymmetric and does not include ram air inlets or a burble fence. The IAD mass properties were determined using sizing relationships presented by Clark et al.[4] and the mass moment of inertia properties were estimated. Table 1 contains geometric, mass, and mass moment of inertia properties for both bodies with the geometry definition given in Figure 2.

In order to add a rotational degree of freedom between the aeroshell and the IAD, they are treated as separate bodies that are attached to each other at a single point. Both bodies remain independently rigid and therefore compatibility between the perimeter of the aeroshell and the IAD is not enforced. The interface is modeled as a spring-damper which constrains the relative motion of the two bodies. Figure 3 illustrates the flexible configuration at an arbitrary pitch difference between the two bodies.

B. Equations of Motion

The equations of motion of the vehicle are derived in the body-fixed coordinate frames attached to each body with the origins coincident at the attachment point. For each body, the pitch angles are defined as positive above the local horizon (see Fig. 1). Figures 4 and 5 illustrate the forces and moments acting on each individual body at the attachment point as well as the definition of both body axes of the system.

Assumptions made in deriving the equations of motion are as follows:

1) The system has four independent degrees of freedom: u, w, θ, and $\Delta\theta$.
2) The x-z and x'-z' planes are coplanar and all motion is constrained to these planes.
3) The center of mass of the aeroshell is fixed but may be offset from the aeroshell's centerline.
4) The center of mass of the IAD is fixed on the IAD's centerline.
5) The attachment between the IAD and the aeroshell is modeled as a single point (i.e., points C and C' in Figs. 4 and 5 are coincident).
6) The planet is flat.
7) There is no wind.
8) The acceleration of gravity, g, is constant.

The translational equations of motion as derived from Newton's second law at a point other than the center of mass are[5]

$$-F_A + R_x - mg\sin\theta = m\left(\dot{u} + Qw + \dot{Q}z_{CM} - Q^2 x_{CM}\right) \tag{1}$$

$$-F_N + R_z + mg\cos\theta = m\left(\dot{w} - Qu - \dot{Q}x_{CM} - Q^2 z_{CM}\right) \tag{2}$$

$$-F_A' + R_X' - m'g\sin\theta' = m'\left(\dot{u}' + Q'w' - Q'^2 x_{CM}'\right) \tag{3}$$

$$-F_N' + R_z' + m'g\cos\theta' = m'\left(\dot{w}' - Q'u' - \dot{Q}'x_{CM}'\right) \tag{4}$$

It is desirable to eliminate the interface forces from the translational equations of motion because they are forces internal to the aeroshell/IAD system. This can be accomplished by recognizing that

$$R_x^{'} = -R_x \cos\left(\theta - \theta^{'}\right) - R_z \sin\left(\theta - \theta^{'}\right) \tag{5}$$

$$R_z^{'} = +R_x \sin\left(\theta - \theta^{'}\right) - R_z \cos\left(\theta - \theta^{'}\right) \tag{6}$$

Substituting Eqs. (5) and (6) into Eqs. (3) and (4) allows the interface force to be removed from the translational equations of motion by solving the resulting system of equations. Rearranging the resulting equations yields the translational equations of motion for the aeroshell as

$$\dot{u} = \frac{1}{m\cos\left(\theta - \theta^{'}\right)} \begin{Bmatrix} -F_A^{'} - \left[F_A + mg\sin\theta + m\left(Qw + \dot{Q}z_{CM} - Q^2 x_{CM}\right)\right]\cos\left(\theta - \theta^{'}\right) \\ -\left[F_N - mg\cos\theta + m\left(\dot{w} - Qu - \dot{Q}x_{CM} - Q^2 z_{CM}\right)\right]\sin\left(\theta - \theta^{'}\right) \\ -m^{'} g\sin\theta^{'} - m^{'}\left(\dot{u}^{'} + Q^{'} w^{'} - Q^{'2} x_{CM}^{'}\right) \end{Bmatrix} \tag{7}$$

$$\dot{w} = \frac{1}{m\cos\left(\theta - \theta^{'}\right)} \begin{Bmatrix} -F_N^{'} + \left[F_A + mg\sin\theta + m\left(\dot{u} + Qw + \dot{Q}z_{CM} - Q^2 x_{CM}\right)\right]\sin\left(\theta - \theta^{'}\right) \\ -\left[F_N - mg\cos\theta + m\left(-Qu - \dot{Q}x_{CM} - Q^2 z_{CM}\right)\right]\cos\left(\theta - \theta^{'}\right) \\ +m^{'} g\cos\theta^{'} - m^{'}\left(\dot{w}^{'} - Q^{'} u^{'} - \dot{Q}^{'} x_{CM}^{'}\right) \end{Bmatrix} \tag{8}$$

The two equations for $\dot{u}^{'}$ and $\dot{w}^{'}$ can be obtained by recognizing that at the attachment point between the aeroshell and the IAD

$$\mathbf{v}_C = \mathbf{v}_{C'} \tag{9}$$

$$\frac{d}{dt}\mathbf{v}_C = \frac{d}{dt}\mathbf{v}_{C'} \tag{10}$$

By carrying out the derivatives on both sides of Eq. (10) and expressing the aeroshell body axis acceleration in the IAD coordinate frame, the translational equations of motion for the IAD are

$$\dot{u}^{'} = \left(\dot{u} + Qw\right)\cos\left(\theta - \theta^{'}\right) + \left(\dot{w} - Qu\right)\sin\left(\theta - \theta^{'}\right) - Q^{'} w^{'} \tag{11}$$

$$\dot{w}^{'} = -\left(\dot{u} + Qw\right)\sin\left(\theta - \theta^{'}\right) + \left(\dot{w} - Qu\right)\cos\left(\theta - \theta^{'}\right) + Q^{'} u^{'} \tag{12}$$

where the velocity of the IAD, written in terms of the velocity of the aeroshell, is

$$u^{'} = u\cos\left(\theta - \theta^{'}\right) + w\sin\left(\theta - \theta^{'}\right) \tag{13}$$

$$w^{'} = -u\sin\left(\theta - \theta^{'}\right) + w\cos\left(\theta - \theta^{'}\right) \tag{14}$$

Equations (11) and (12) can be substituted into Eqs. (7) and (8), yielding the two degree of freedom equations of motion in translation in the aeroshell body-fixed frame.

The rotational equations of motion for the aeroshell and the IAD are taken about the coincident origins of the body-fixed frames and are given by

$$M_R + M_{aero,C} - mg\left(x_{CM}\cos\theta + z_{CM}\sin\theta\right) = \dot{Q}\left[I_{yy} + m\left(z_{CM}^2 + x_{CM}^2\right)\right] - mx_{CM}\dot{w} + mz_{CM}\dot{u} + mQ\left(wz_{CM} + ux_{CM}\right) \tag{15}$$

$$-M_R + M_{aero,C'} - mgx_{CM}^{'}\cos\theta^{'} = \dot{Q}^{'}\left[I_{yy}^{'} + m^{'} x_{CM}^{'2}\right] - m^{'} x_{CM}^{'}\dot{w}^{'} + m^{'} Q^{'} u^{'} x_{CM}^{'} \tag{16}$$

By rearranging Eqs. (15) and (16), the rotational rate equations of motion for the aeroshell and the IAD are given by

$$\dot{Q} = \frac{M_R + M_{aero,C} - mg\left(x_{CM}\cos\theta + z_{CM}\sin\theta\right) + mx_{CM}\dot{w} - mz_{CM}\dot{u} - mQ\left(wz_{CM} + ux_{CM}\right)}{I_{yy} + m\left(z_{CM}^2 + x_{CM}^2\right)} \tag{17}$$

$$\dot{Q}' = \frac{-M_R + M_{aero,C'} - m'gx'_{CM}\cos\theta' + m'x'_{CM}\dot{w}' - m'Q'u'x'_{CM}}{I'_{yy} + m'x'^2_{CM}} \tag{18}$$

M_R is the interface moment between the aeroshell and IAD. For this derivation the interface moment will be modeled as a torsion spring and damper of the form

$$M_R = -\kappa\left(\theta - \theta'\right) - \eta\left(Q - Q'\right) \tag{19}$$

The explicit form of the equations of motion given by Eqs. (7), (8), (17), and (18) are obtained by casting the equations in matrix form and solving for the state variable time derivatives. Doing so yields the equations of motion as a function of the state variables *u, w,* Q, Q', θ, and θ'. The equations of motion for the pitch angle of both bodies are

$$\dot{\theta} = Q \tag{20}$$

$$\dot{\theta}' = Q' \tag{21}$$

Because the calculation of atmospheric density requires the altitude of the vehicle as input, another equation of motion is required to obtain the vertical location of the vehicle from the surface of the planet in inertial space. This equation can be obtained by resolving the body-fixed velocity components of the aeroshell vertically using the equation

$$\dot{h} = u\sin\theta - w\cos\theta \tag{22}$$

C. Atmospheric Model

The calculation of density is accomplished using an exponential model which is a curve fit of data from the descent of the Viking Lander.[6] The model has the general form

$$\rho(h) = \rho_0 \exp\left(-\frac{h}{H}\right) \tag{23}$$

where in the Martian case the reference density, ρ_0, is 0.0216 kg/m^3 and the scale height, *H*, is 9.76 km.

D. Aerodynamics

The aerodynamics of both the aeroshell and the IAD were calculated using modified Newtonian aerodynamics. While this method of analysis is typically reserved for the hypersonic regime of flight, the aerodynamics of an isotensoid IAD remain roughly constant through the supersonic regime as it approaches the hypersonic limit.[1] Therefore it is assumed that this method for determining the aerodynamics of the IAD remains valid in the supersonic regime spanning Mach 2.5 to 5. Comparison of modified Newtonian aerodynamic results for the isotensoid shape with experimental data[3] verifies the validity of this assumption.

Aerodynamic moments for both bodies are calculated about the attachment point *C/C'*. The reference area and length used are the projected area and diameter, respectively, for each body (see Figure 2). Note that the calculated aerodynamic forces and moments for the IAD do not include the depicted flat front panel, but the only external curved boundary. The aerodynamic moment coefficient trend with respect to angle of attack for both bodies indicates they are both statically stable about the point *C/C'* (see Table 2). The coefficient of both moment and normal forces with respect to angle of attack are linear within the range of interest. Axial forces are a function of

angle of attack for both bodies with the maximum value at zero angle of attack indicated in Table 2. The value for base pressure coefficient was set to zero during the aerodynamic analysis. Equation (24) expresses the calculation of total aerodynamic moment due to static and dynamic aerodynamics.

$$M_{aero} = \left[C_{m_\alpha} \alpha + C_{m_Q} \frac{Qd}{2V} \right] S d q_\infty \tag{24}$$

The effect of pitch damping derivatives (i.e., C_{m_Q}) are included in this study. For this analysis, pitch damping is assumed to be constant (i.e., not varying with angle of attack) for each body. The stable (i.e., negative) value of pitch damping is obtained using modified Newtonian aerodynamics. For the unstable value of pitch damping, the sign of the stable result was changed from negative to positive. Neutral (i.e., zero) pitch damping is used by default in this analysis with the effects of stable and unstable pitch damping determined in a parametric study for the free flight case.

E. Non-dimensionalization of Interface Quantities

Non-dimensionalization of the interface stiffness and damping makes it easier to interpret the results. The interface stiffness is non-dimensionalized using static aerodynamics while the interface damping is non-dimensionalized according to the damping ratio found in literature.[7] The non-dimensional interface stiffness is given by the equation

$$\hat{\kappa} = -\frac{\kappa}{C_{m_\alpha} q_{\infty,0} (S' + S) d'} \tag{25}$$

where the denominator represents an effective stiffness due to aerodynamic forces. The aerodynamic moment coefficient is that of the combined bodies about the attachment point. The dynamic pressure is the initial value for the problem being investigated. The reference area and length are the projected area and diameter of the entire vehicle. Therefore, Eq. (25) provides a transformation from the dimensional spring stiffness to a non-dimensionalized stiffness for a given geometry and initial flight condition.

Non-dimensionalizing the interface damping is achieved by using the damping ratio, defined as

$$\hat{\eta} = \frac{\eta}{2\sqrt{\kappa I_{eff}}} \tag{26}$$

where the denominator is the critical damping for a torsion spring.[8] The effective moment of inertia is related to the relative oscillation mode between the aeroshell and the IAD as they oscillation in a vacuum. The effective moment of inertia is defined to be

$$I_{eff} = \left(1 - \frac{I_{yy}}{I_{yy} + I'_{yy}} \right) I_{yy} \tag{27}$$

Substituting Eq. (27) into Eq. (26) yields the non-dimensional spring damping. Note that the presence of the spring stiffness in the non-dimensional damping term causes a correlation between the selections of the two non-dimensional quantities. This correlation could be avoided by non-dimensionalizing the damping against a relevant non-zero value of C_{m_Q} (e.g. its value at zero angle of attack).

III. Results

A. Simulation Validation

In order to compare the behavior of the multibody free flight simulation to already-existing solutions, the non-dimensional interface stiffness and damping were set arbitrarily high to cause the vehicle to behave as a single

rigid body. The numerically integrated angle of attack history of the vehicle was compared to a closed form solution[2] for a Mars flight case. Both analyses yielded identical results.

B. Constant Velocity Results

In this modification to the free flight case, a virtual thrust is applied at the attachment point to counteract the drag experienced by both bodies at a particular instant. By adding this virtual thrust, the vehicle is allowed to have a steady airspeed after the initial transients are passed. Because a virtual thrust is used instead of a virtual sting, the vehicle is still allowed to heave. The effect of gravity is also removed from the simulation leaving only the effects of the interface and aerodynamics. The initial conditions for the simulation are given in Table 3 with the density being held constant. Each case was run for five seconds.

Stability regimes for the constant velocity simulation are obtained by isolating the longest period motion of the angle of attack of the aeroshell with respect to time. For each run representing a unique combination of $\hat{\kappa}$ and $\hat{\eta}$, a curve fit is applied to the numerical results of the aeroshell angle of attack time history. Because for some interface designs there is a secondary, short-period oscillation, the nonlinear curve fit must have the form

$$\alpha(t) = A_1 e^{B_1 t} \cos(\omega_1 t + \phi_1) + A_2 e^{B_2 t} \cos(\omega_2 t + \phi_2) \tag{28}$$

The exponential decay constant corresponding to the longer period motion (i.e., the ω_1 or ω_2 with lower value) is used in the constant velocity case as a measure of stability. Acceptable fits were determined to be those with a coefficient of determination to the numerical results in excess of 0.99.

Figure 6 shows contours of the decay constant over a large range of non-dimensional interface stiffness and damping values for $C_{m_Q} = 0$. Two major regions of stability associated with the constant velocity case can be discerned. While both regions are characterized by statically stable behavior, the region spanning high non-dimensional interface stiffness values exhibits dynamic instability of the aeroshell angle of attack as time progresses (i.e., $B > 0$). In the other region, the angle of attack amplitude of the aeroshell is dynamically stable (i.e., $B < 0$) and therefore decays as time progresses. As designs move toward the interior of this region, B becomes increasingly negative and thus the time history of aeroshell angle of attack becomes more highly damped.

C. Free Flight Results

The free flight simulation reflects the behavior of the vehicle as it decelerates in the Martian atmosphere while under the influence of the planet's gravity field. The initial conditions for this case are given in Table 4 and the simulation was terminated once Mach 2.5 was reached or the angle of attack of either the aeroshell or the IAD exceeded 30 degrees.

Figure 7a qualitatively shows three distinct regions of stability associated with the free flight case for $C_{m_Q} = 0$. The region that spans high values of non-dimensional interface stiffness is characterized by statically stable, dynamically unstable oscillation of the aeroshell angle of attack. This is the same behavior as observed in the constant velocity simulation at high non-dimensional interface stiffness values. In the region spanning moderate non-dimensional interface stiffness values there is statically stable oscillation of aeroshell angle of attack which decays to a lower amplitude with respect to the beginning of the simulation. This behavior is defined as being statically and dynamically stable. In the region encompassing low non-dimensional interface stiffness values, the aeroshell is initially driven to angles of attack exceeding 30 degrees. For this analysis such behavior is defined as being divergent, even though for some cases the aeroshell angle of attack may return to lower values due to the restoring influence of aerodynamic and interface moments when the system oscillations grow to large amplitudes.

The effect of gravity is negligible in the behavior of the system as removing gravity did not affect the stability boundaries seen in Fig. 7a. Applying a stable pitch damping ($C_{m_Q} < 0$) to both bodies had the effect of removing the boundary separating the dynamically stable and unstable regions for the ranges of $\hat{\kappa}$ and $\hat{\eta}$ considered and replacing it with a single region of static and dynamic stability as seen in Fig. 7b. As non-dimensional interface stiffness is decreased the aeroshell stability is dominated by the effect of the drag of the IAD. As such, applying a stable pitch damping did not affect the boundary between the statically and dynamically stable region and the divergent region. Applying an unstable pitch damping ($C_{m_Q} > 0$) to both bodies had the effect of lowering the boundary between the statically stable but dynamically unstable and the statically and dynamically stable regions as

seen in Fig. 7c. Again, the boundary between the statically and dynamically stable region and the divergent region remains unaffected due to the dominance of the IAD drag at low values of non-dimensional interface stiffness.

D. Stability Mechanisms

All cases discussed in this section have neutral pitch damping ($C_{m_Q} = 0$). With high values of the non-dimensional interface stiffness the aeroshell and IAD exhibit statically stable but dynamically unstable trends of aeroshell and IAD angle of attack as shown in Fig. 8. This behavior is observed both in the constant velocity and free flight simulations. For the constant velocity simulation, the generation of lift causes dynamically unstable behavior due to the heaving the vehicle. For the free flight case, both the generation of lift and the decreasing dynamic pressure cause dynamically unstable behavior.[2]

Reducing the non-dimensional interface stiffness has the effect of creating statically and dynamically stable angle of attack time histories for the aeroshell and IAD. In this region, the vehicle interface is a dominant factor in the stability of the vehicle. Figure 9 shows such a case from the free flight simulation. The difference in aerodynamic moment between the aeroshell and the IAD induces an initial difference in pitch and pitch rate between the bodies. The lag in pitch rate activates the damping mode of the interface causing dissipation of rotational energy from the system. This dissipative effect can be removed if non-dimensional interface stiffness is held constant and the non-dimensional interface damping is reduced significantly, as shown in Fig. 10. Without the effect of interface damping, the same dynamically destabilizing effects as observed in the highly stiff limit are once again dominant.

The region of divergent behavior is observed only in the free flight case where both the non-dimensional interface stiffness and damping have low values. Figure 11 shows a case in this region from the free flight simulation. When the non-dimensional interface stiffness and damping are in this region, the two bodies are given significant freedom to initially rotate independently of each other. Because the aerodynamic moment acting on the IAD is much greater than that acting on the aeroshell, the IAD quickly rotates into the oncoming flow and oscillates about an angle of attack of zero while the aeroshell remains at a positive angle of attack. The drag force of the IAD is transmitted to the aeroshell through the interface with an angular bias with respect to the aeroshell centerline. As the aeroshell center of mass is located on the centerline behind the attachment point, a pitch-up moment is experienced by the aeroshell. Figure 12a shows the components of the moments on the aeroshell about its center of mass for the case in Fig. 11. Because the moment due to the drag of the IAD becomes stronger than the aeroshell's combined aerodynamic and reaction moments, the aeroshell angle of attack diverges. This can be verified by Fig. 12b, which gives the sum of all the moments in Fig 12a. Note that this behavior is not witnessed in the constant velocity simulation due to the addition of the drag-countering virtual thrusts to each body.

IV. Conclusions

This paper has presented the equations of motion for a four degree of freedom vehicle consisting of an aeroshell with an attached IAD. Using these equations, along with aerodynamic data generated by numerical computation, the effect of varying the non-dimensional interface stiffness and damping on vehicle stability was determined. It was shown that, depending on the combination of non-dimensional interface stiffness and damping, the effects on the static and dynamic stability of the aeroshell can be significant. For high values of the non-dimensional interface stiffness the system behaves as a single rigid body and exhibits the characteristic statically stable but dynamically unstable time history of the angle of attack of rigid bodies. For moderate values of non-dimensional interface stiffness, the system exhibits statically and dynamically stable behavior of aeroshell angle of attack due to the dissipating effect of the interface damping. For low values of interface stiffness, the system exhibits divergent behavior of aeroshell angle of attack due to the biased pointing of the IAD drag force.

While no provision has been made in this study to determine physically realistic values of non-dimensional interface stiffness and damping, the framework developed is able to accommodate such data. If provided with specific values of stiffness and damping, the simulation will predict the stability behavior of the vehicle during flight. Therefore, when combined with a fluid-structure interaction code, this simulation framework is a useful tool for evaluating the stability of IAD designs.

Acknowledgments

The research presented in this paper was supported under a Graduate Research Assistantship funded by NASA Langley Research Center through the National Institute of Aerospace. Support was also provided by the Program to Advance Inflatable Decelerators for Atmospheric Entry (PAIDAE).

References

[1]Gillis, C. L., "Deployable Aerodynamic Decelerators for Space Missions," *AIAA Journal of Spacecraft and Rockets*, Vol. 6, No. 8, 1969, pp. 885-890.

[2]Schoenenberger, M., Queen, E. M., "Limit Cycle Analysis Applied to the Oscillations of Decelerating Blunt-Body Entry Vehicles," *NATO RTO Applied Vehicle Technology Panel Symposium*, RTO-MP-AVT-152, Loen, Norway, 2008.

[3]Mikulas, M. M., Bohon, H. L., "Development Status of Attached Inflatable Decelerators," *AIAA Journal of Spacecraft*, Vol. 6, No. 6, 1969, pp. 654-660.

[4]Clark, I. G., Hutchings, A. L., Tanner, C. L., Braun, R. D., "Supersonic Inflatable Aerodynamic Decelerators for Use on Future Robotic Missions to Mars," *IEEE Aerospace Conference*, IEEEAC paper #1419, Big Sky, Montana, 2008.

[5]Baruh, H., *Analytical Dynamics*, WCB/McGraw-Hill, New York, 1999.

[6]Seiff, A., "Post-Viking Models for the Structure of the Summer Atmosphere of Mars," *Advances in Space Research*, Vol. 2, No. 2, 1982, pp. 3-17.

[7]Nashif, A. D., Jones, D. I. G., Henderson, J. P., *Vibration Damping*, John Wiley & Sons, New York, 1985. p. 132.

[8]Jacobsen, L. S., Ayre, R. S., *Engineering Vibrations with Applications to Structures and Machinery*, McGraw-Hill, New York, 1958, p. 394.

Table 1. Mass and geometry properties of the aeroshell and IAD. Coordinate systems for center of mass location are defined in Figures 4 and 5.

Parameter	Aeroshell	IAD
m	2648 kg	29 kg
I_{yy}	2863 kg-m^2	294 kg-m^2
d	4.5 m	10.18 m
S	15.9 m^2	65.5 m^2
x_{CM}	-0.44 m	-2.66 m
z_{CM}	0.00 m	Not Applicable

Table 2. Predicted aerodynamic quantities for the aeroshell and IAD.

Parameter	Aeroshell	IAD
C_{m_α}	-0.2007 rad^{-1}	-0.3881 rad^{-1}
C_{N_α}	0.2761 rad^{-1}	0.7786 rad^{-1}
C_{m_Q}	-0.360 rad^{-1}	-0.311 rad^{-1}
	0	0
	0.360 rad^{-1}	0.311 rad^{-1}
Max C_A	1.5498	0.7675

Table 3. Initial conditions for constant velocity simulation.

Parameter	Value
M	4.5
α, α'	5 deg
θ	0 deg
$\Delta\theta$	0 deg
ρ	2.78×10^{-3} kg/m^3
Q, Q'	0 deg/sec

Table 4. Initial conditions for free flight simulation.

Parameter	Value
M	5
α, α'	5 deg
θ	0 deg
$\Delta\theta$	0 deg
h	20 km
Q, Q'	0 deg/sec

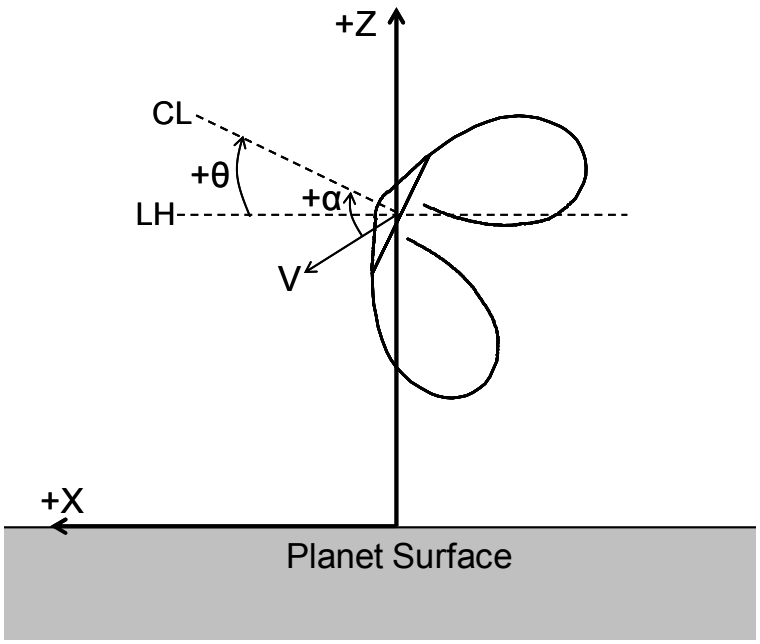

Figure 1. Aeroshell with isotensoid IAD in flight.

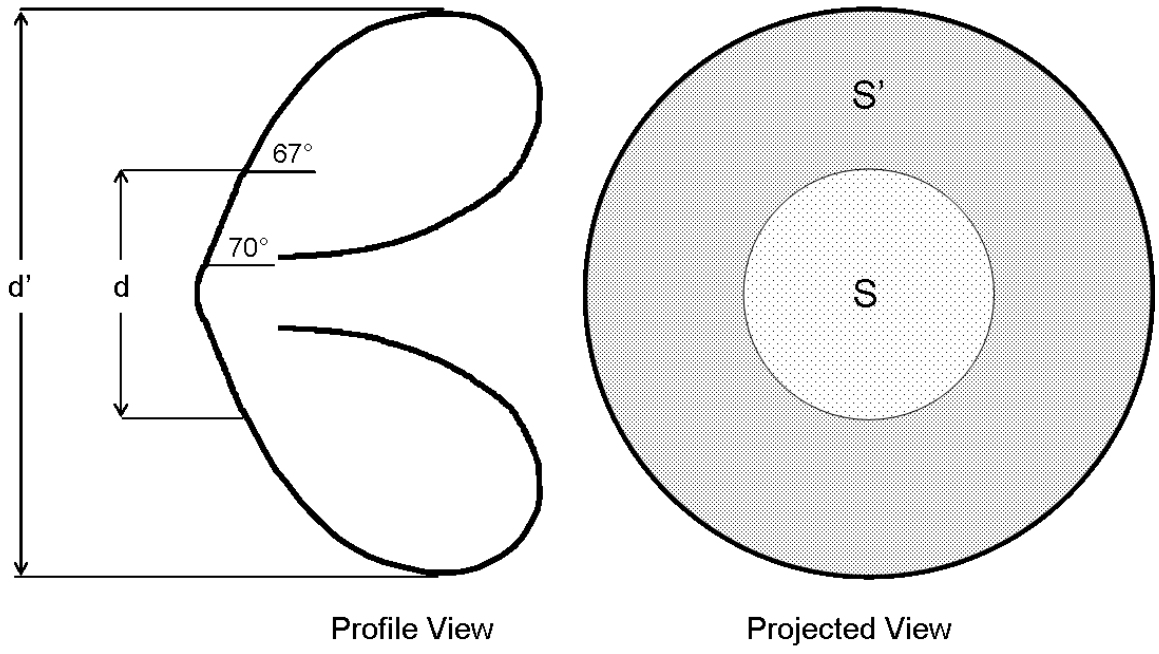

Figure 2. Geometry definition for the aeroshell and IAD.

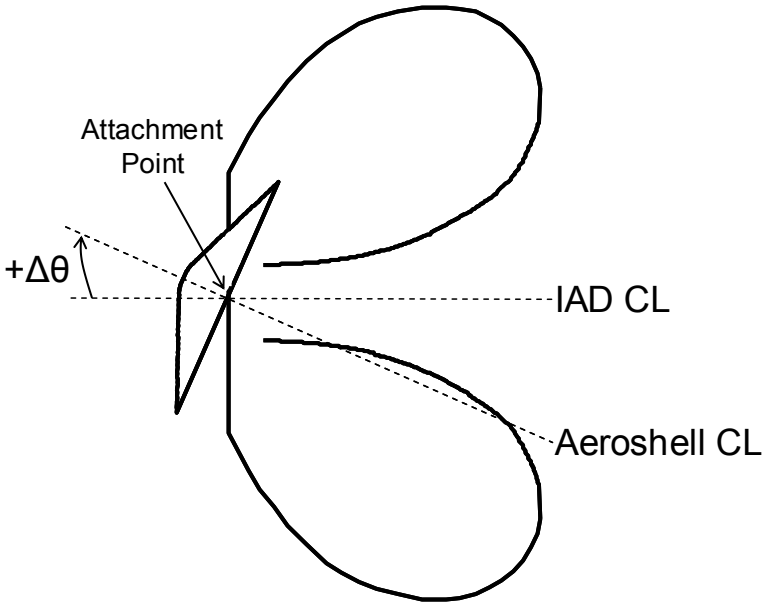

Figure 3. Flexible aeroshell and IAD system. Moments due to the spring and damper at the interface point depend on the relative angle and its time derivative, respectively.

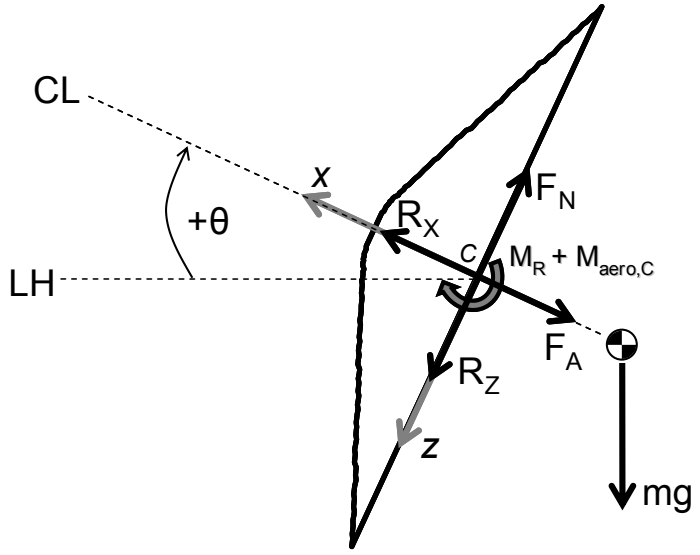

Figure 4. Aeroshell with external forces, interface forces and moments, and coordinate system definition.

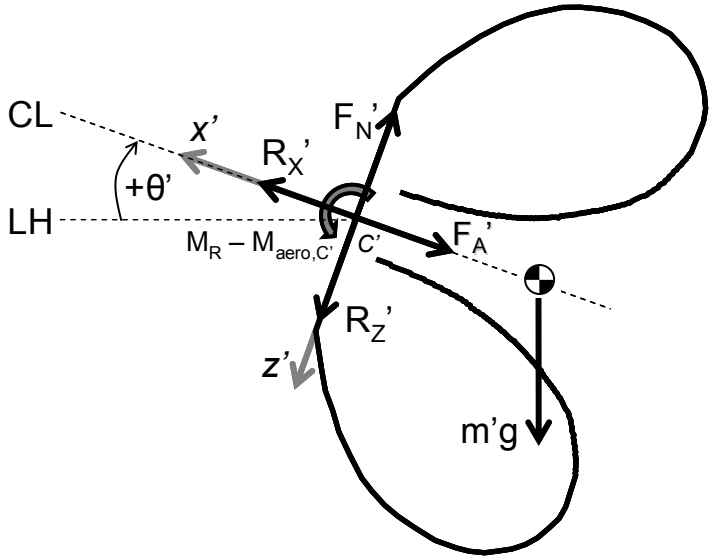

Figure 5. IAD with external forces, interface forces and moments, and coordinate system definition.

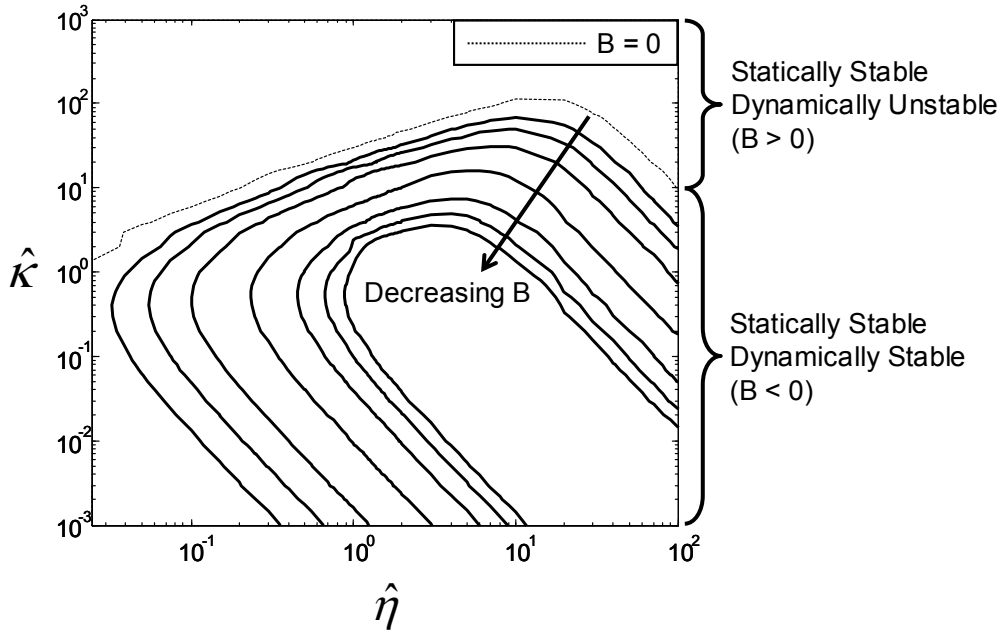

Figure 6. Contours of the decay constant, B, are shown as a function of non-dimensional interface stiffness and damping with $C_{m_Q} = 0$.

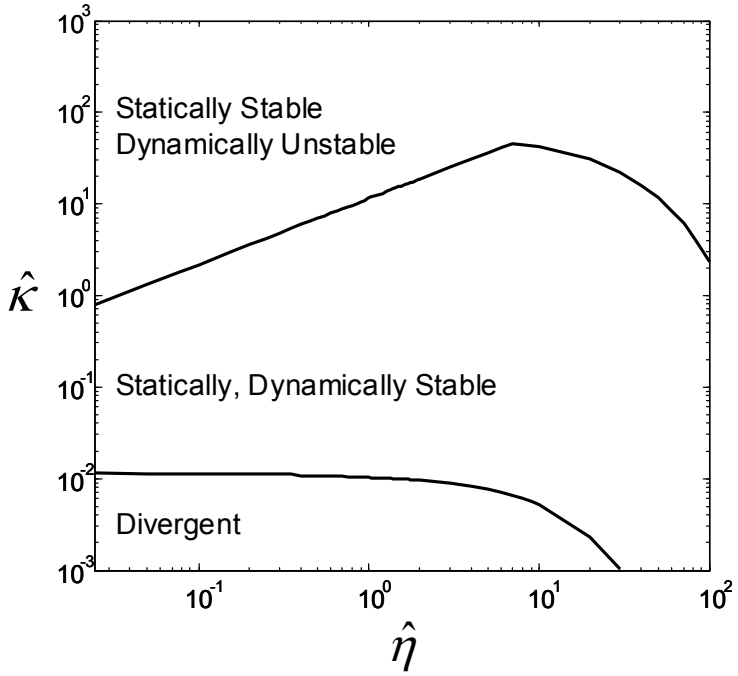

Figure 7a. Qualitative stability regimes for aeroshell angle of attack in free flight with $C_{m_Q} = 0$.

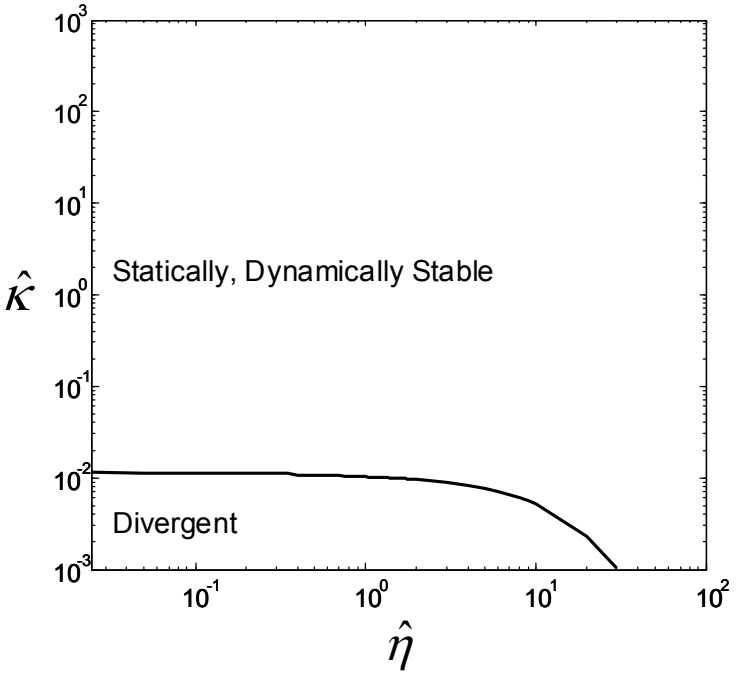

Figure 7b. Qualitative stability regimes for aeroshell angle of attack in free flight with $C_{m_Q} < 0$.

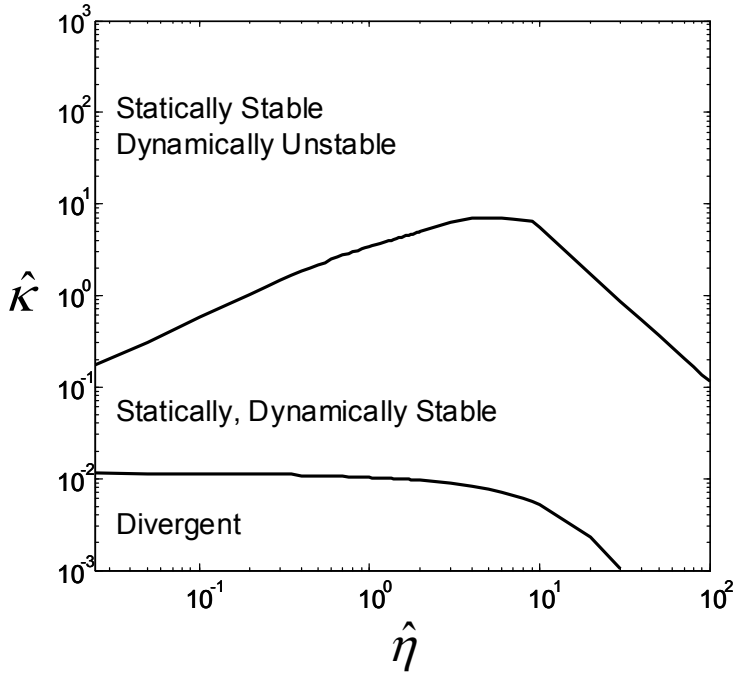

Figure 7c. Qualitative stability regimes for aeroshell angle of attack in free flight with $C_{m_Q} > 0$.

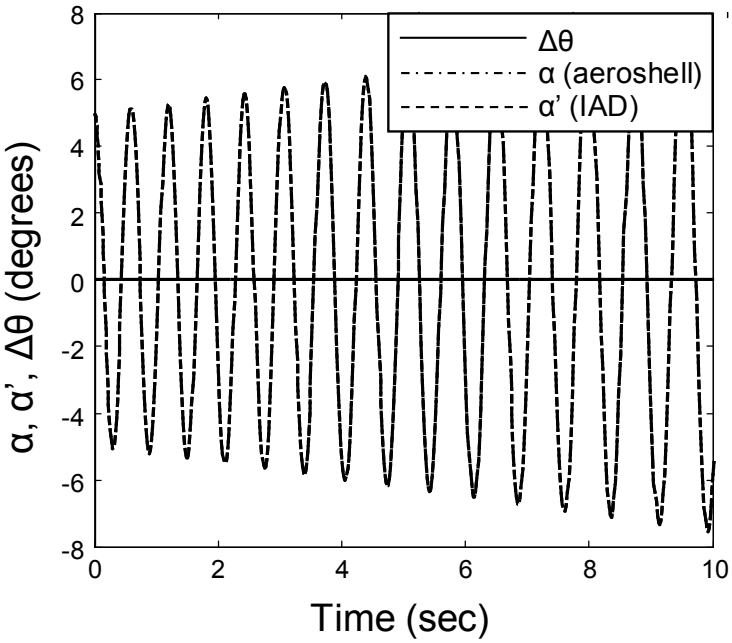

Figure 8. Statically stable but dynamically unstable angle of attack oscillation trends for free flight case with $\hat{\kappa} = 1000$, $\hat{\eta} = 2$, $C_{m_Q} = 0$. Note that the time history of angle of attack for the aeroshell and IAD are the same and that $\Delta\theta$ remains at zero.

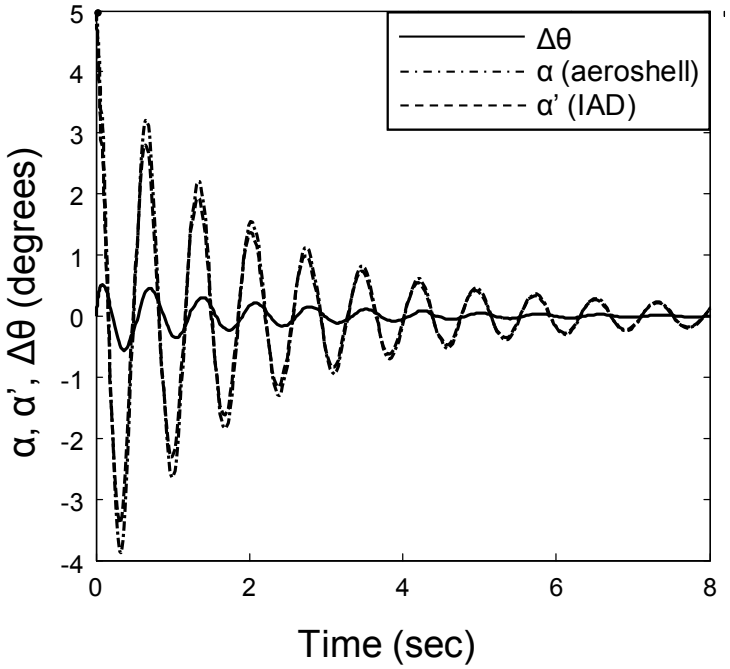

Figure 9. Statically and dynamically stable angle of attack oscillation trends for free flight case with $\hat{\kappa} = 3,\ \hat{\eta} = 2,\ C_{m_Q} = 0$.

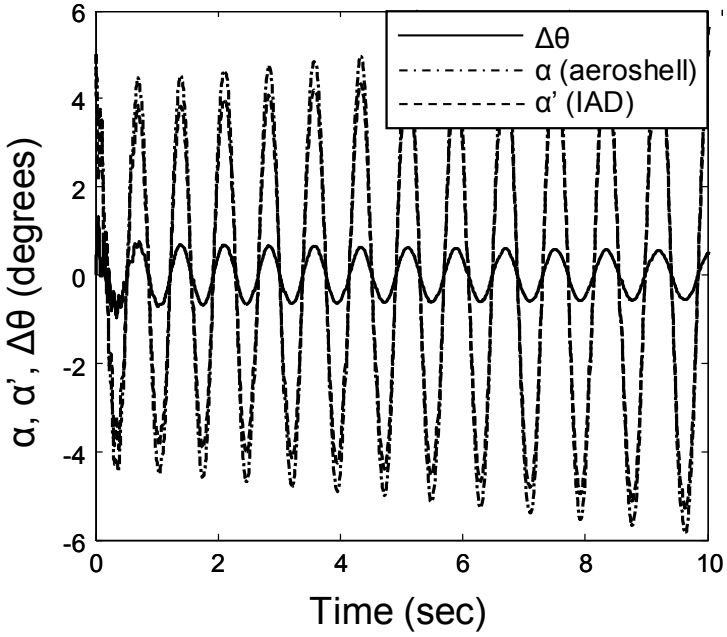

Figure 10. Statically stable but dynamically unstable angle of attack oscillation trends for free flight case with $\hat{\kappa} = 3,\ \hat{\eta} = 0.05,\ C_{m_Q} = 0$.

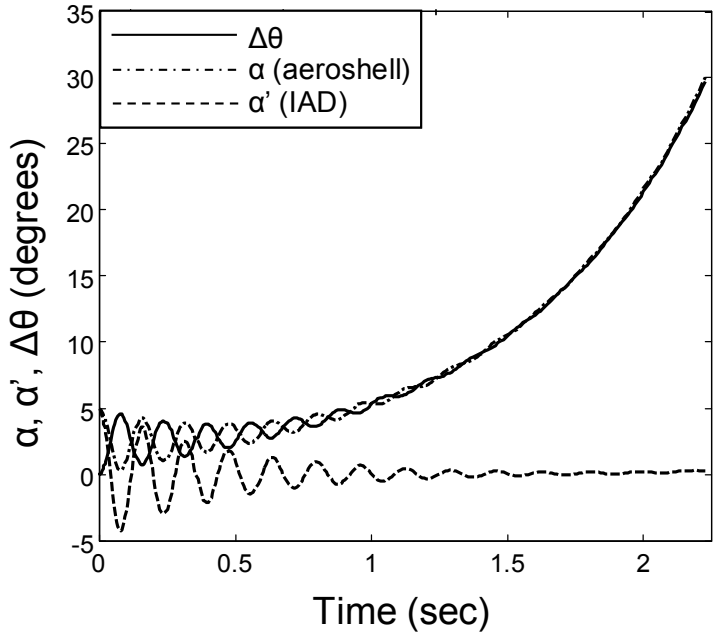

Figure 11. Divergent aeroshell angle of attack oscillation trend for free flight case with $\hat{\kappa} = 0.001,\ \hat{\eta} = 2,\ C_{m_Q} = 0$.

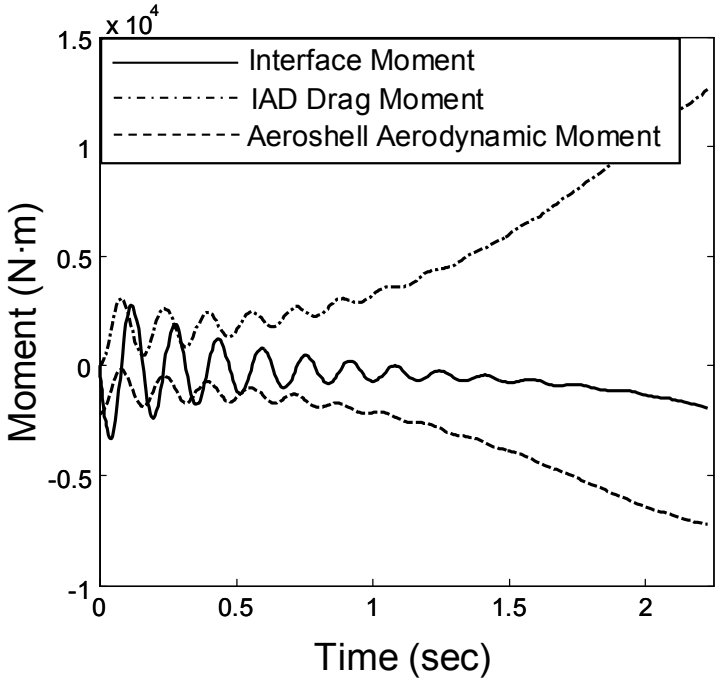

Figure 12a. Components of the moment about the aeroshell center of mass for a free flight case with $\hat{\kappa} = 0.001,\ \hat{\eta} = 2,\ C_{m_Q} = 0$. The moment due to gravity is neglected.

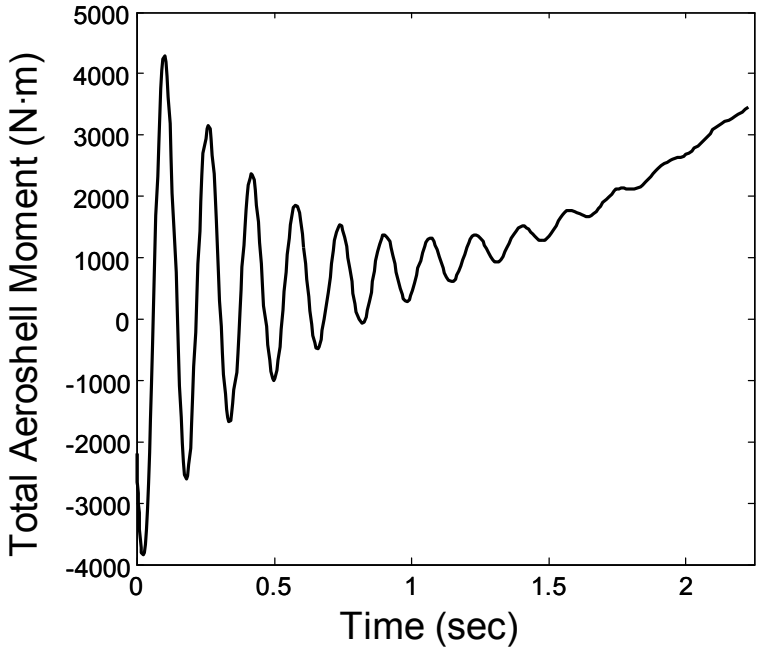

Figure 12b. Total moment about the aeroshell center of mass for a free flight case with $\hat{\kappa}$ = 0.001, $\hat{\eta}$ = 2, $C_{m_Q} = 0$. The moment due to gravity is neglected.